Effect of prior austenite grain size on the abrasive wear resistance of ultra-high strength martensitic steels

Oskari Haiko[1*], Vahid Javaheri[1], Kati Valtonen[2], Antti Kaijalainen[1], Jaakko Hannula[1], Jukka Kömi[1]

[1] Materials and Mechanical Engineering, Centre for Advanced Steels Research, University of Oulu, Finland
[2] Tampere Wear Center, Materials Science and Environmental Engineering, Tampere University, Finland

[*]Corresponding author. Email address: oskari.haiko@oulu.fi, (O. Haiko)

Abstract

Prior austenite grain size has a marked effect on the hardenability, strength, and impact toughness properties of steels. This study was conducted in order to understand the effect of prior austenite grain size and morphology on the mechanical properties and abrasive wear performance of an ultra-high strength steel. A commercial quenched 500 HB grade wear-resistant steel was selected for the study: the steel was austenitized at two different temperatures and compared to the original, as-received quenched condition. The resulting mean prior austenite grain size was ranging from 14 µm to 34 µm. The decrease in grain size improved the low-temperature impact toughness properties. A high stress abrasive wear testing method with natural granite abrasives was utilized for the evaluation of abrasive wear resistance. The results suggest that decreasing the prior austenite grain size improves the abrasive wear resistance with similar hardness level martensitic steels. In addition, high-resolution electron backscatter diffraction measurements revealed formation of ultra-fine grain structures in the severely deformed regions of the wear surfaces.

1. Introduction

Steels are commonly used as wear-resistant materials in different applications across various industrial sectors. Often steels are the most cost-efficient material solution for wear-resistant purposes due to the desirable mechanical properties and the ease and scale of production. In abrasive environments, the quenched and tempered martensitic steels are perhaps the most commonly utilized steel grades. Martensite phase shows high hardness and strength, which both can be adjusted by alloying and different heat treatments [1]. Modern steelmaking and thermomechanical controlled processing have enabled the production of ultra-high hardness steels with leaner alloying and lower energy consumption [2]. Novel processing routes, such as direct-quenching and direct-quenching and partitioning, can be used to fabricate high-hardness steels without the need for subsequent heat treatments [3–6]. These methods are also applied in the production of wear-resistant steels.

Prior austenite grain size (PAGS) has a well-known effect on the strength and impact toughness of martensitic steels. The famous Hall-Petch equation [7,8] has been one of the most profound discoveries in understanding the mechanical properties of steels. Decreasing the prior austenite grain size results in finer sub-structure in martensitic steels, which leads to increased strength, and also improves the impact toughness, especially in low temperature range [9,10]. Nowadays the thermomechanical controlled processing and hot rolling below non-crystallization regime are used

for refining the grain structure to improve strength and impact toughness [4,11]. The alteration of the grain structure and morphology is often considered essential for achieving ultra-high strength properties for medium-carbon steels. Apart from increasing the yield strength and improving the toughness properties, the prior austenite grain size may also affect the work-hardening capability of steels due to the changes in dislocation density; decreasing the prior austenite grain size has been seen to increase the dislocation density of martensitic steels [12]. However, most studies involving austenitization and different PAGS give no comparison to deformed, elongated structures with different austenite morphology from the equiaxed grain structure.

Wear-resistant steels have been studied intensively to understand the relationship between the microstructure, mechanical properties and wear resistance [6,13–16]. Hardness has long been considered the general property that determines the wear resistance of steels, especially when testing steels with similar microstructure and different hardness levels, e.g. martensitic steels with different carbon content [17]. However, different microstructures have been shown to exhibit distinct wear behavior [18,19], and also martensitic steels with similar hardness level have been found to exhibit differences in terms abrasive wear resistance [14,20]. Also, fracture toughness has been shown to have a significant effect the wear resistance of steels [21,22]. Moreover, the work-hardening capability of martensitic steels, when subjected to heavy abrasive or impact-abrasive wear, has been one of the major subjects of some recent studies. Research work by Haiko, Valtonen and Ojala et. al. [6,14,20] have suggested that work-hardening capability is an essential feature determining the wear performance of steels when testing in high-stress abrasive conditions. In an review by Chintha [23], it was pointed out that very limited amount of studies has been published on understanding the effect of work-hardening on the abrasive or impact-abrasive wear resistance of martensitic steels. Also, the effect of prior austenite grain size or morphology on the work-hardening of steels during abrasion or impact wear is of little knowledge. Therefore, the current study has been conducted in order to understand the effect of prior austenite grain size on the abrasive wear resistance of martensitic steels.

2. Materials and methods

The commercial 500 HB wear-resistant steel was received as heavy sheet plate (abbreviated C27) and was cut to smaller plates (300 mm x 250 mm x 6 mm) suitable for heat treatment in laboratory furnace. The nominal chemical composition of the investigated steel is presented in Table 1. Two different austenitization temperatures (860 and 960 °C) were used for altering the prior austenite grain size. Holding time for the austenitization was 25 min. After heat treatment, the test plates were quenched in water with high cooling rate (>80 °C). In addition to the reheated and quenched steel variants, C27 steel in the as-received quenched state was included. Therefore, total of three material variants were tested. The materials were named C27-DQ for the C27 in the as-received condition, C27-860 and C27-960 indicating the subsequent heat treatment temperatures, respectively.

Table 1
Chemical composition of the tested steel showing the nominal maximum content, from product brochure (wt.%, balance Fe).

Material	C	Si	Mn	Cr	Mo	Ni	B
C27	0.27	0.50	1.60	1.20	0.25	0.25	0.005

Mechanical testing included tensile tests, Charpy-V notch test for impact toughness properties, and hardness testing for bulk material and wear surface. Three specimens were tested per material for tensile strength. The samples were cut transverse to the rolling direction with reduced sample section dimensions of 6 mm x 20 mm x 120 mm. The tensile testing was done with MTS-810 universal

servohydraulic testing machine. Charpy-V impact toughness measurements (ISO 148-1) were made for three samples per material and the testing was conducted at -40 °C with sample dimensions of 6 mm x 10 x 55 mm. Hardness was measured through the thickness of the samples with minimum of 10 indentations using Vickers HV10 method. CSM Instruments MHT-Z-AE microhardness tester was used for measuring the hardness of the wear surfaces. Indentations were made with 0.25 N force and three series of five indentations were made on different locations on the wear sample surfaces.

Wear tests were performed in Tampere Wear Center (TWC) at Tampere University, Finland. An in-house, pin-mill type tester was utilized for the wear testing (Fig. 1). Referred as the dry-pot tester, the device has been used extensively for testing the abrasive wear resistance of steels and can be used with both dry abrasive bed [20,24,25], like in this study, and with slurry [16,26]. The tester has two main parts: the rotating shaft with sample holders and a steel pot, in which the abrasive media is placed. The samples travel through the gravel bed when the shaft is rotated. The rotation speed was set at 250 rpm producing 2.5 m/s speed when measured from the tip of the samples. The testing time was 240 min consisting of four 60 min periods during which four samples were tested simultaneously. One of the samples was a 400 HB reference material for monitoring the test and the three other samples were the three variants of the C27 steel. Two rounds of complete 240 min tests were done, i.e. two samples per each material variant were tested. The typical standard deviation of the method is less than 4 % [15]. Natural granite sieved to 8–10 mm size distribution from Kuru quarry, Finland, was selected as the abrasive media and the 9000 g batch of granite was replenished for every 60 min period for fresh, sharp abrasives. Moreover, for every test period, 1350 g of 100–600 µm quartzite was placed below the granite bed to prevent the flow of larger abrasives under the rotating shaft. The sample position was changed for every period to have similar wear conditions for all samples. The order of the sample positions was reversed for the second round of testing. The sample dimensions were 64 x 40 x 6 mm and the samples were set at +45° angle to the normal.
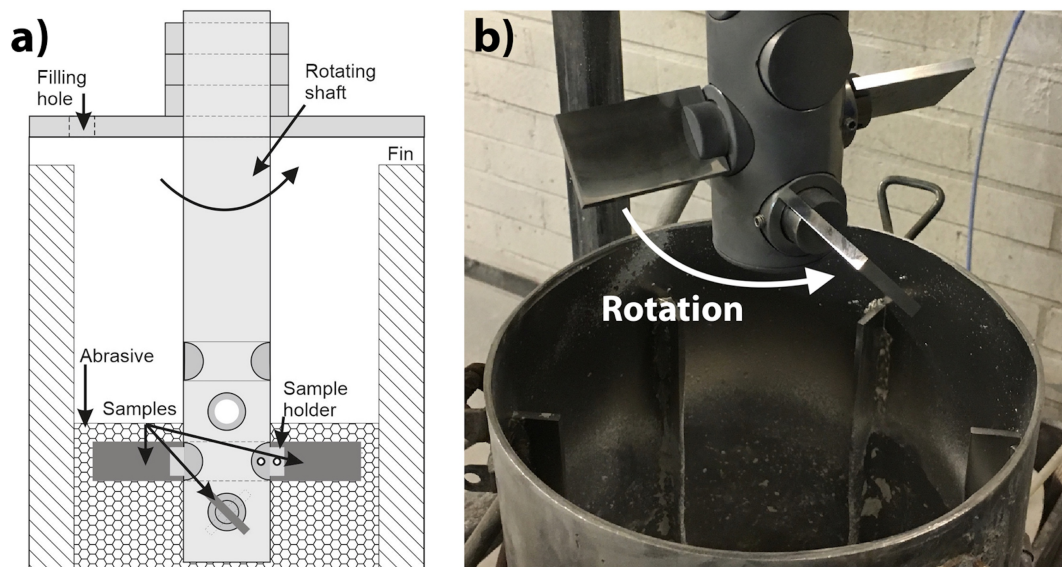
Fig. 1. a) Schematic illustration of the high-stress abrasive tester (dry-pot) and b) image of the tester with four samples fitted at + 45° angle.

Optical, laser scanning confocal (Keyence VK-X200) and field-emission scanning electron microscopes (FESEM, Zeiss Sigma,) were utilized for the characterization of the microstructures and the wear surfaces. The cross-sectional (Fig. 2, section c) samples were prepared by polishing and etching with 2 % Nital prior to microscopy. Tapered samples were prepared at an angle of 10° to horizontal for inspection of the worn surfaces from above in addition to the cross-sectional views. Similar sample preparation method has been used earlier by Valtonen et al. [20].
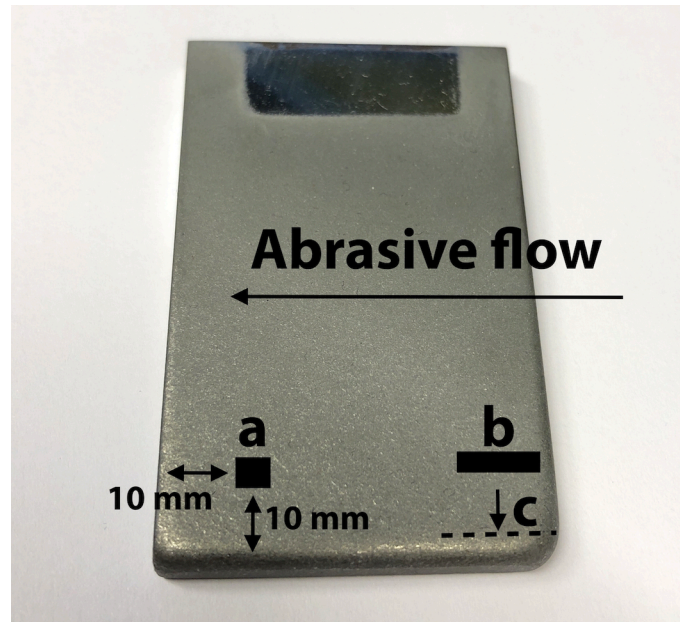
Fig. 2. Dry-pot sample after wear testing marked with locations for the respective measurements (not in true scale): a) surface roughness, b) BSE imaging area (three images), and c) cross-sectional sample cutting direction (dashed line) and inspection direction (arrow). Abrasive flow during testing also shown.

Prior austenite grain sizes were measured from laser scanning micrographs with a calculation tool introduced by Seppälä et al. [27] from planar sections taken from rolling-to-normal (RD-ND) direction at quarter thickness of the plates. The samples for PAGS were etched in a saturated aqueous solution of picric acid along with a few drops (3-4 drops) hydrochloric acid. Five images per sample were examined for the PAGS calculations that included minimum of 400 grain boundary intercepts. In order to have more information concerning the prior austenite structure, on the basis of orientation relations between the parent austenite and the final microstructure (as the product of quenching), a reconstruction technique was applied to the electron backscatter diffraction (EBSD, Zeiss Sigma) data using Matlab supplemented with the MTEX toolbox [28–30]. The worn and heavily deformed samples were coated with nickel to improve the measurement quality of the EBSD mapping. The polishing method for the EBSD samples was adopted from the work of Stechow et al. [31]. Different magnifications and step sizes were used for the imaging and analysis.

The laser scanning confocal microscope was also used for the surface profile roughness measurements (R_a, arithmetic mean roughness and R_q, root mean square height) based on the ISO 4287-1997 standard. Values were measured on an area of 3.4 mm x 2.3 mm located 10 mm from the edges of the samples (Fig. 2, section a) and three measurements were done for each sample. The granite surface coverage was calculated from the backscatter electron (BSE) images (Fig. 2, section b) with the help open-source Fiji image processing package based on ImageJ analysis software, and three images per sample were analyzed. Rikagu SmartLab 9 kW X-ray diffractometer (XRD) with cobalt K_α radiation anode was used for detecting any retained austenite. The results of XRD measurements were analyzed with PDXL2 software with the Rietveld's whole powder fitting method. Samples for the XRD analysis were cut from the as-received and heat-treated test plates, ground to quarter thickness from the surface of the samples prior to polishing with colloidal silica suspension.

3. Results

3.1. Microstructures of the studied steels

The steel microstructures were fully martensitic with some effects of autotempering visible. FESEM images of the tested steels are given in Fig. 3. Images were obtained at the quarter depth of the samples. The steels showed some precipitates, which indicates that autotempering had taken place during the quenching. These white precipitates were presumably transition carbides formed during the quenching process when autotempering occurred [1]. The martensite start temperature (M_s) was estimated to be around 360–380 °C (Andrews linear and product [32]), which would have meant some time for the autotempering to take place even with high cooling rates. The C27-DQ in the received condition showed slightly more contrast between the dark, untempered martensite and the precipitate rich areas, which indicated that possibly some low-temperature tempering could have been applied. Retained austenite content was measured with the XRD and the results revealed that the C27-DQ and C27-960 had less than 1.0 % austenite retained in the matrix, whereas the C27-860 had 2.5 % austenite still present.
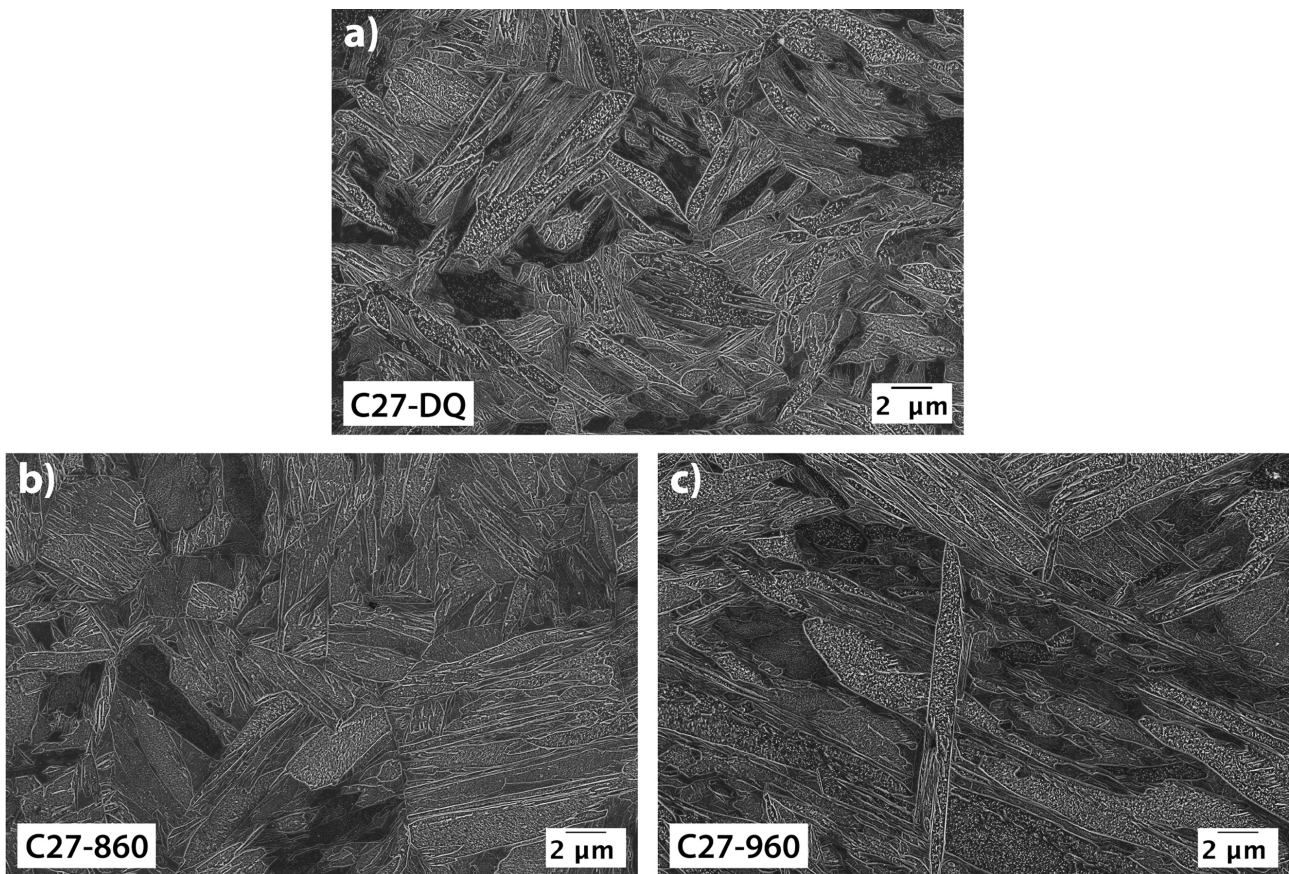

Fig. 3. Typical microstructures of the studied steels.

3.2. Prior austenite grain size and morphology

The prior austenite grain sizes measured from planar sections taken in rolling-to-normal (RD-ND) direction are presented in Table 2, and laser scanning confocal images of the picric acid etched samples are shown in Figs. 4a-c along with grain size distribution. The C27 steel showed distinguishably different prior austenite grain size for all three variants. The largest PAGS was measured for the sample austenitized at 960 °C. The two other C27 variants showed almost similar
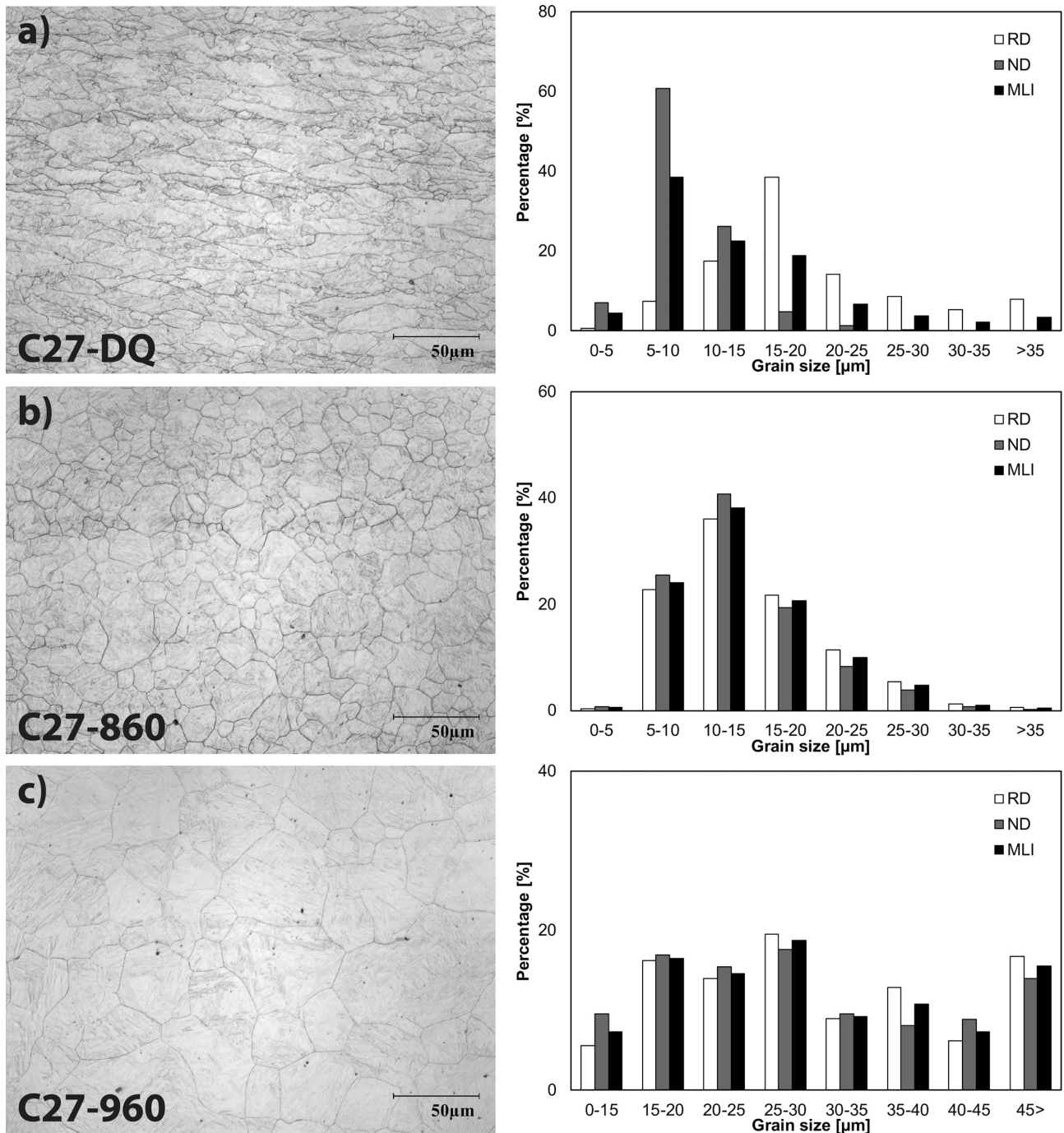
mean linear intercept (MLI), but the grain morphology and aspect ratio were different. The C27-DQ had elongated, "pancaked" grain structure that had been presumably been produced by hot-rolling below non-recrystallization temperature region, i.e. thermomechanical controlled processing had been applied. In contrast, the C27-860 showed more equiaxed grain structure due to the austenitization. It should be noted that both of the reheated variants of the C27 had similar, elongated grain structure (Fig. 4a) prior to the austenitization as the C27-DQ in the as-received condition had.

Table 2
Prior austenite grain sizes of the tested steels: L_1 for the rolling direction (RD), L_2 for the normal direction (ND) and mean linear intercept (MLI) with standard deviations and calculated aspect ratio.

| Material	L_1 (RD) [µm]	L_2 (ND) [µm]	Aspect ratio	MLI [µm]
C27-DQ	21.5 ± 9.8	9.2 ± 2.9	2.33	13.7 ± 8.6
C27-860	14.9 ± 6.2	13.9 ± 5.7	1.07	14.5 ± 6.0
C27-960	35.0 ± 16.0	33.3 ± 13.8	1.05	34.3 ± 15.1

The grain size distribution is also shown in Fig. 4. The mean linear intercept gives an estimation of the average grain size, but the distribution is more relevant for analyzing the grain structure. For the C27-DQ, most of the grains in the rolling direction (RD) were longer than 20 µm and some grains were measured larger than 35 µm in length. However, there were basically no grains larger than 20 µm in the normal direction (ND) while most of the grains were in the 5-10 µm size range. Therefore, the MLI set to around 15 µm due to the elongated structure. The C27-860 had grain size more evenly distributed and most grains were in the size range of 10-15 µm with nearly equiaxed grains. The aspect ratio was close to 1 also for the C27-960, but the grain size distribution was more heterogenous compared to C27-860. Some large grains were visible, and there was almost the same amount of grains in the size range of 20 to 25 µm as there were grains larger than 45 µm.

Fig. 4. Prior austenite grain structure revealed by picric acid etching (left) and grain size distribution for both directions (RD, ND) and mean linear intercept (MLI) (right).

EBSD was also carried out for the further inspection on the prior austenite grain size. A Matlab code with the help of MTEX toolbox, originally developed by Nyyssönen [33] and later modified by Javaheri [29], was employed for the recreation of the grain boundary images from the EBSD data of the final microstructure. Although only one measurement was performed for each sample, the results were in quite good agreement with the picric acid etching results (see Table 2). Fig. 5 shows the reconstructed parent austenite structures that revealed a drastic difference for the PAGS of the samples, indicating a randomly oriented grain structures in all specimen. The details for the grain size distribution (on the basis of calculated equivalent circle diameter for each grain) show slightly finer grain size distribution for the C27-860 compared to the C27-DQ. The C27-960 shows very coarse grain structure, such that the maximum grain size was nearly two times larger than the largest

grain in the two other samples. In addition to the grain structure, the EBSD data including the image quality (IQ) mapping showed the sub-structure of the martensitic steels.
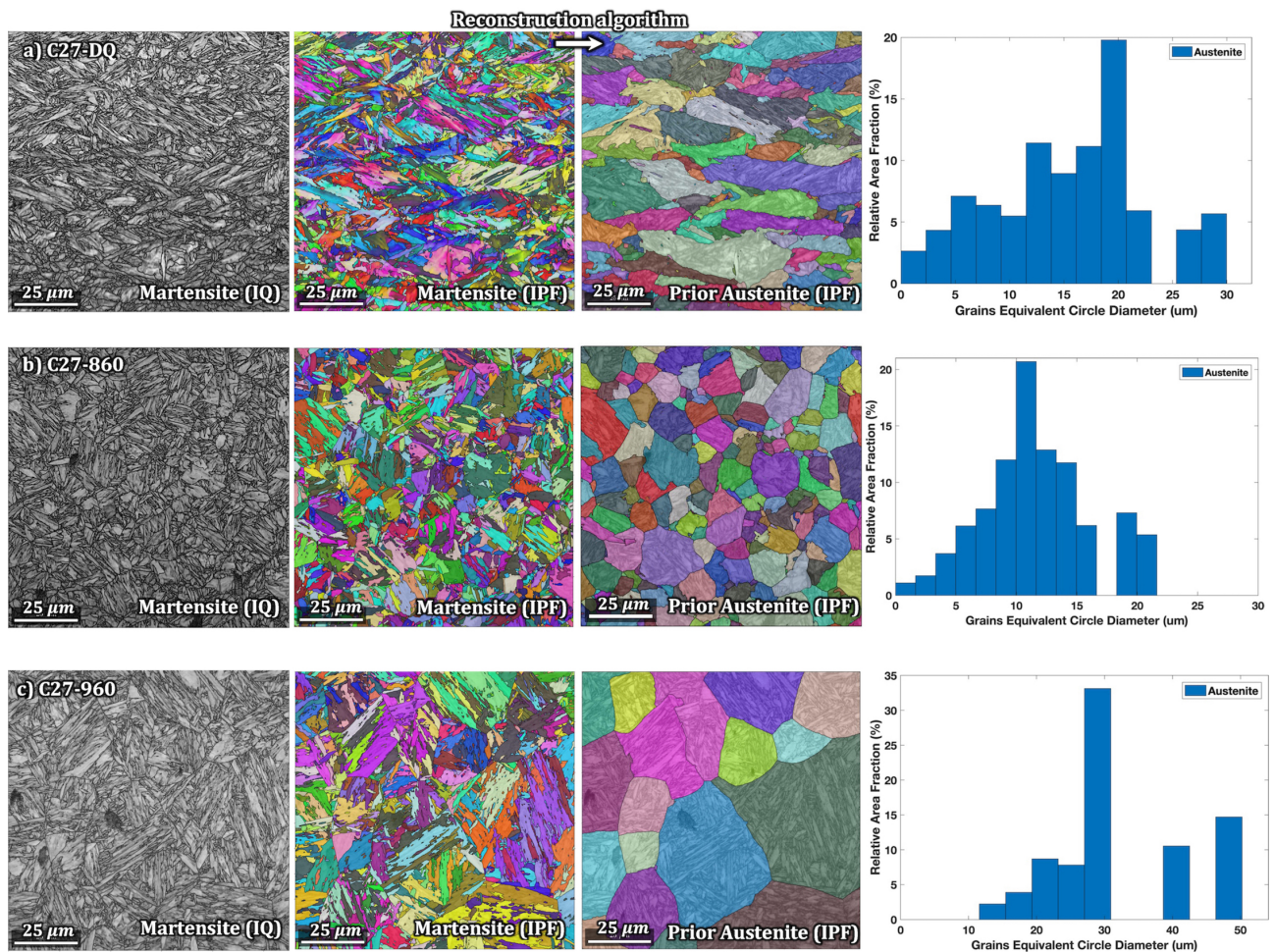
Fig. 5. Reconstructed grain boundary images from the EBSD data (IQ-map on the left, and reconstructed grains on the right): a) C27-DQ, b) C27-860, and c) C27-960; RD-ND direction. The grain size distribution for the samples are also given.

The distribution of calculated equivalent circle diameter (ECD) of the martensite blocks size of the for all three samples are presented in Fig. 5. Coarse prior austenite grain structure produced coarser final microstructure, as expected. The sample C27-860, which had the finest prior austenite grain size, showed also the finest sub-structure such that the martensite blocks were almost distributed normally with an average of 4 μm block size. It should be also remarked that all samples showed a random-oriented grain structure, and there was no specific intense orientation population in the inverse pole figure maps. Hence, it can be assumed that the probable effect of texture had no account on the wear resistance of the examined samples.

3.3. Mechanical properties

Table 3 shows the mechanical properties of the tested steels, including 0.2% offset yield strength ($R_{p0.2}$), ultimate tensile strength (R_m), percentage elongation after fracture (A), bulk Vickers hardness (HV10), and impact toughness tested at -40 °C. The impact toughness test results were converted directly proportional from measured joules to J/cm². In general, the commercial C27 steel showed high strength combined with relatively good impact toughness values at -40 °C. Altering the grain

structure and the prior austenite grain size had the most significant effect on the impact toughness measured with the Charpy-V tests. The C27-860 had the highest impact toughness energies among the tested samples. When comparing the two C27 steels with the equiaxed grain structure, the increase of PAGS from around 14 μm to 34 μm resulted in half the impact energy when tested at -40 °C. Thus, the significance of the grain size for the impact toughness was substantial for the C27 steels.

Table 3
Mechanical properties of the tested steels and retained austenite (RA) content.

Material	$R_{p0.2}$ [MPa]	R_m [MPa]	A [%]	Hardness HV10 [kgf/mm^2]	Charpy-V (-40 °C) [J/cm^2]	RA [%]
C27- DQ	1279 ± 25	1624 ± 31	8.8 ± 0.4	469 ± 8	65 ± 3	<1.0
C27-860	1211 ± 16	1577 ± 15	11.9 ± 0.3	475 ± 8	100 ± 3	2.5
C27-960	1117 ± 10	1510 ± 11	11.5 ± 0.4	455 ± 10	48 ± 3	<1.0

The yield and tensile strength were decreased by the reaustenitization, while the elongation improved. The C27-960 with the largest PAGS had more than 100 MPa lower strength compared to the C27-DQ. The yield-to-tensile strength ratio also decreased slightly for the heat-treated steels. However, hardness was the highest for the C27-860, though only by a small margin, and the differences in the hardness values were quite small. Therefore, the effect of the initial hardness between the steels would be minimized regarding the wear test results. The differences in strength and toughness values between the steels were in a quite good agreement with literature [9,10], when taking in account the change in grain size: strength and toughness decreased with the increasing PAGS.
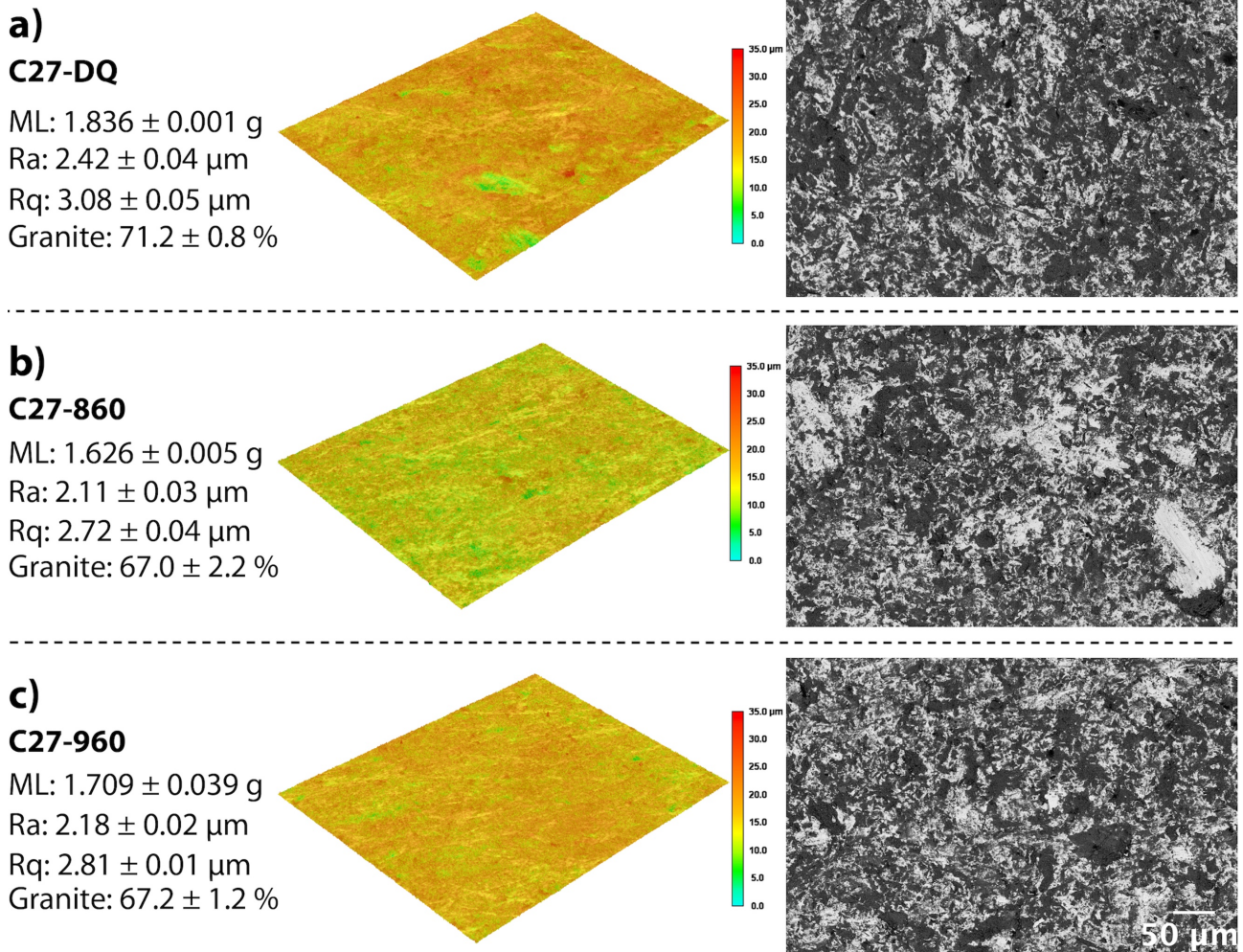

3.4. Wear test results

3.4.1. Mass loss, surface roughness, and granite coverage

The results for the dry-pot wear testing are given in Fig. 6, which also includes surface roughness measurement results and granite covered area in percent. The lowest mass loss (1.626 ± 0.005 g) was measured for the variant austenitized at 860 °C, which also had the highest initial hardness among the C27 steels. However, the differences in the bulk hardness of the steels did not solely explain the wear results: the C27-960 showed lower mass loss (1.709 ± 0.039 g) compared to the C27-DQ (1.836 ± 0.001 g) despite lower initial hardness. Moreover, the hardness difference between C27-DQ and C27-860 was almost within limits of error, but the wear test results had greater difference between the two steels than deviation could explain.

The surface roughness values (R_a and R_q) were measured with the laser scanning confocal microscope. The results were in line with the mass loss with all the tested steels: the higher the mass loss, the higher the surface roughness (see Fig. 6). Generally, some larger pits and craters could be seen with the C27-DQ, while the C27-860 and C27-960 showed more scratches than pits or craters. The C27-DQ with the highest mass loss had slightly higher granite coverage, but the differences between the steels were small. Figure 6 shows examples of 3D-topography maps (surface roughness) and granite coverage (BSE images) along with R_a and R_q and mass loss.

a)

C27-DQ

ML: 1.836 ± 0.001 g
Ra: 2.42 ± 0.04 μm
Rq: 3.08 ± 0.05 μm
Granite: 71.2 ± 0.8 %

b)

C27-860

ML: 1.626 ± 0.005 g
Ra: 2.11 ± 0.03 μm
Rq: 2.72 ± 0.04 μm
Granite: 67.0 ± 2.2 %

c)

C27-960

ML: 1.709 ± 0.039 g
Ra: 2.18 ± 0.02 μm
Rq: 2.81 ± 0.01 μm
Granite: 67.2 ± 1.2 %

Fig. 6. Left: Mass loss (ML) with standard deviation included, surface roughness values (R_a and R_q), granite area coverage, and 3D-topography maps (cropped to 2 mm x 1.5 mm area); a) C27-DQ, b) C27-860, and c) C27-960. Right: BSE images of the worn surfaces of the given samples.

3.4.2. Cross-sections of the wear surfaces

The samples were cut for the cross-sectional study of the wear surfaces (Fig. 7a-c). The images were taken approximately 5 mm from the rounded tip of the sample with laser scanning confocal microscope (see Fig. 2, section c). The depth of the visibly deformed surface was less than 20 μm for all the tested steels. The sub-surface deformation was more in the form of highly deformed and orientated microstructure and only few shear bands were detected. White etching layer had formed in all of the samples, but the layers were mostly concentrated on the edges of the samples, where the most severe wear is present during the testing. The embedment of the granite particles was substantial as seen earlier in the BSE images. Parts of the samples showed tribolayer formation, i.e. mixture of steel and granite. The images only show the two-dimensional aspect of the surface, and therefore it should be borne in mind that the granite particle embedment and penetration beneath the surface may cover larger areas than actually visible in the images.
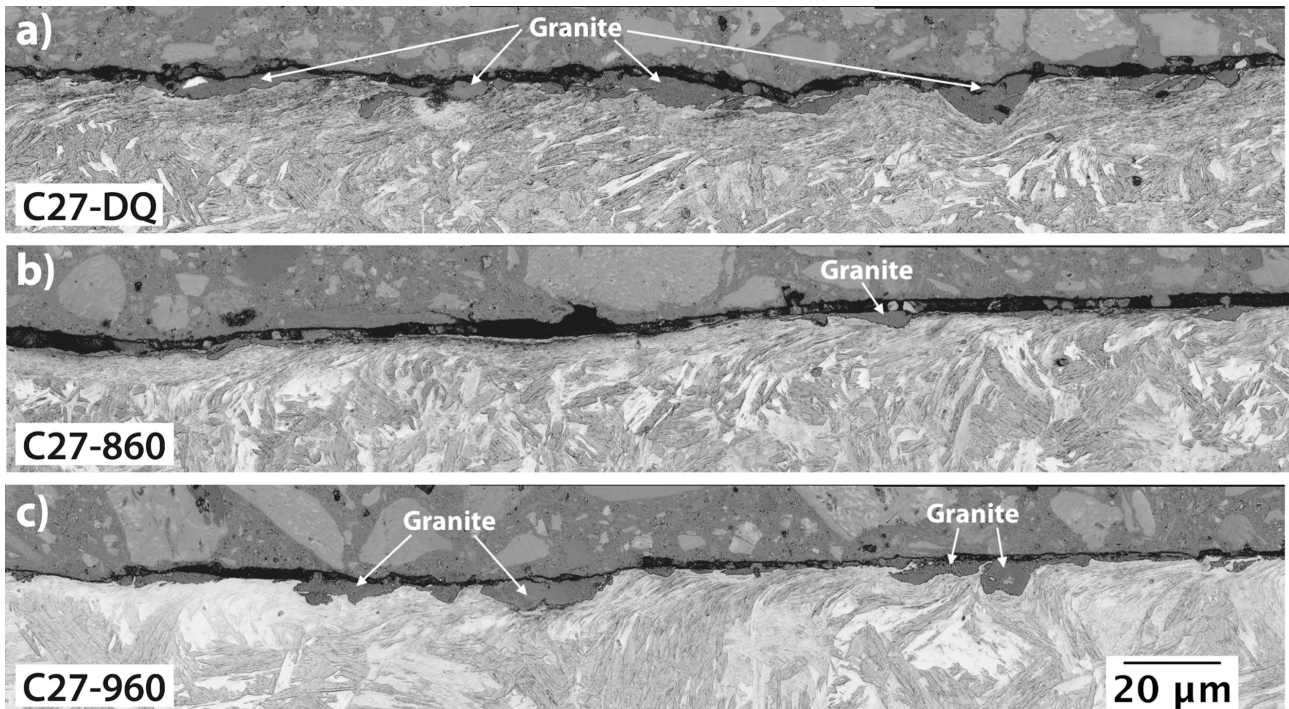
Fig. 7. Laser scanning confocal panorama images of the cross-sections of the wear surfaces: a) C27-DQ, b) C27-860, and c) C27-960. Abrasive flow direction from left to right.

Further inspection with FESEM imaging was conducted for more in-depth analysis of the worn samples (Figs. 8a-c). The orientation of the laths had turned into the direction of the granite particle flow, which is typical for martensitic steels in dry-pot testing [20]. The fibered and orientated laths are the result of heavy deformation and the direction of the abrasive flow can be seen (left to right). The wear test samples had experienced a large degree of plastic deformation and extensive tribolayer formation had occurred; the tribolayer being visible better in the FESEM images compared to the laser scanning images. The penetration of hard granite particles had caused the surface to deform considerably creating a mixture of steel and granite on the surface that was especially thick in C27-DQ (Fig. 8a). Considering the material removal and mass loss during the testing, this tribolayer was then eventually removed by the continues ploughing by the abrasives. Microcutting and microploughing had taken place, but the general view of the surface suggested that the steels did not appear to have behaved in a brittle manner, i.e. extensive surface fracture did not occur. As a summary of the wear process, the constant flow of the abrasive granite particles inflicted damage on the surface by the aforementioned mechanisms of microploughing and further microcutting, and finally caused the material to be removed.
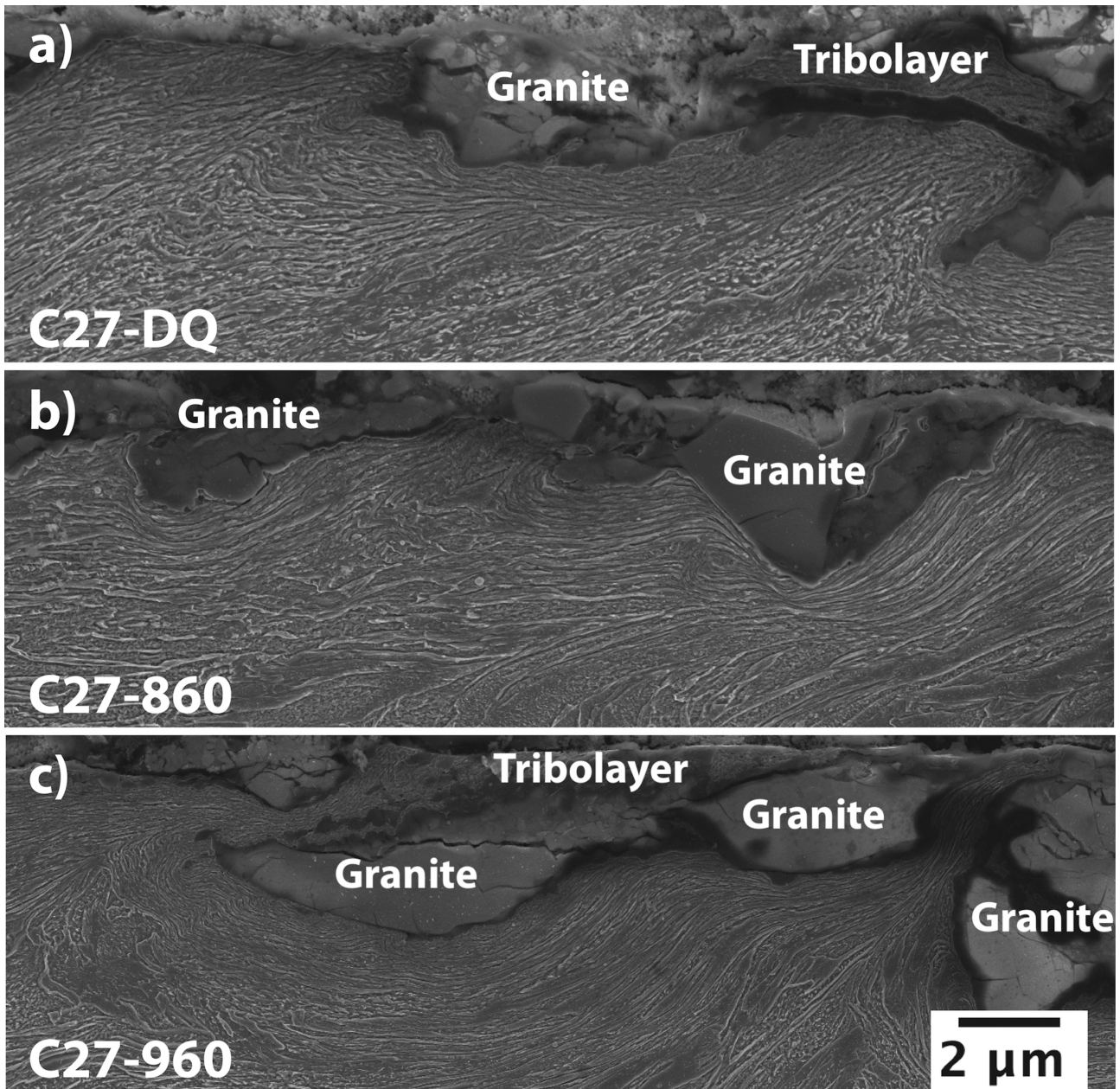
Fig. 8. FESEM close-up images of wear surfaces a) C27-DQ, b) C27-860, and c) C27-960.

3.4.3. Tapered surfaces and microhardness measurements

Fig. 9 shows the tapered sections with the granite-steel interface: in the images the grey area is the surface of the sample and the lighter area is the steel sample. The abrasive flow was from top to bottom in the images. Some white etching layer can be seen extending from the surface to a depth of few microns. Differences between the steels were quite small, but the general observation was that the granite particle penetration was slightly deeper for the C27-DQ and C27-960 compared to the C27-860. The inspection of the wear surface from above shows how the granite particles have attached to the surface and created pit-like pools beneath the surface surrounded by heavily deformed microstructure. The combination of the 2D-images from two directions (from the side Figs. 7 and 8, and above Fig. 9) gives some insight on the abrasive particle penetration and microstructure deformation. As a result, it can be presumed that the granite-steel tribolayer creates a complex interface that acts as pathway for cracks. The properties of this layer have significant effect on the

wear resistance. However, it is still somewhat difficult to interpret whether the tribolayer could act as protective layer or decrease material removal rate.
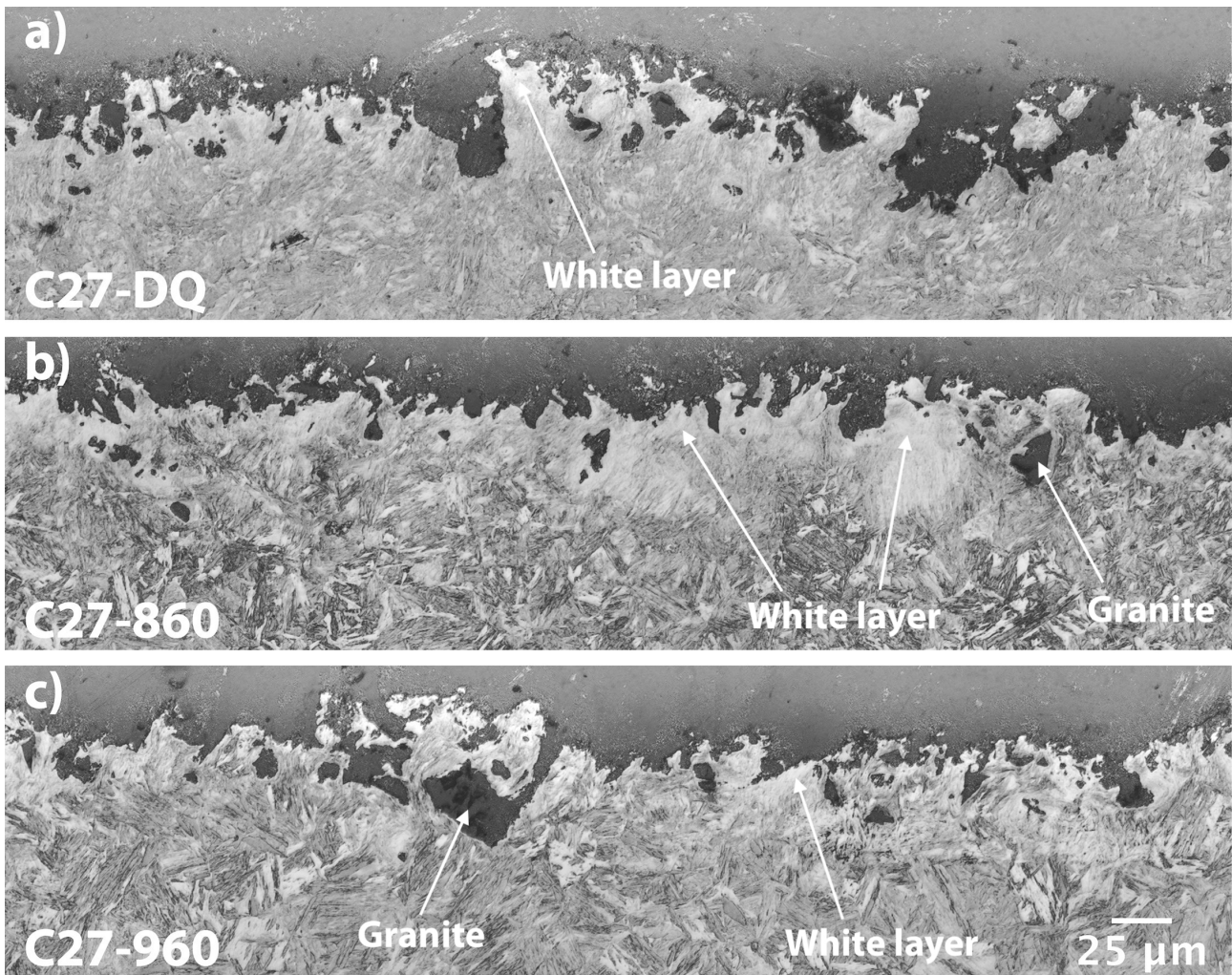
Fig. 9. Laser-optical images of the worn surface of the tapered samples.

The tapered sections were also used for microhardness testing to evaluate the work-hardening of the steels. The indentations were made as close as possible to the wear surface near the interface between the steel and the granite layer. The deviation was high for the hardness measurements due to the extreme local deformation of the steels and due to the low load used in the measurements (0.25 N). The average microhardness values of the deformed surface were 589 ± 22 HV (C27-DQ), 793 ± 63 HV (C27-860), and 602 ± 38 HV (C27-960), respectively. The microindentations revealed that the hardness had increased drastically; an indication of strong work hardening presumably caused by the extreme grain refinement on the wear surface. The work-hardened layer of the C27-860 reached over 300 HV increase over the initial bulk hardness, which was the highest for the tested steels. The other two C27 steels also showed increased hardness for the deformed layer, but that was not as substantial as with the C27-860. Fig. 10 shows the correlation between the hardness of the deformed surface and mass loss.
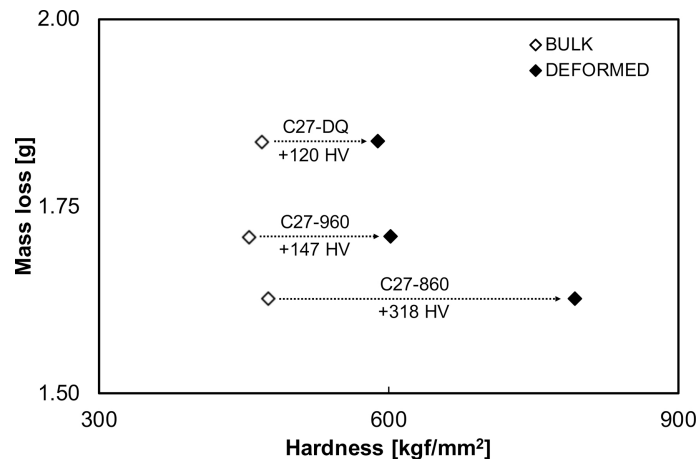
**Fig. 10.** Mass loss and deformed hardness.

3.4.4. EBSD analysis

The EBSD analysis was employed for further investigation of the wear surfaces. As an example of the results, the image quality along with the inverse pole figure map for two different magnifications for the sample C27-960 are presented in Fig. 11. Several attempts have been made to either do or improve the EBSD measurements of highly deformed surfaces and microstructures [31,34–37]. Hence, the quality of the obtained data is improving. Here, in this work, it was possible to capture the EBSD data with a high confidence index from even the ultra-fine structure of the wear surfaces due to some considerations as using nickel coating for the examined samples, special sample preparation method with small amount of load but for longer time, and with very accurate focusing during the measurements.

The damaged zone visible in the EBSD images consisted of two distinguished regions: i) a narrow severely deformed layer near the tribological layer, which was darker in the IQ image than for the rest of the microstructure, probably due to higher dislocation density at this region, and then slightly further ii) highly deformed layer which appeared almost as light as the undeformed layer. Fig. 12 shows the image quality of the damaged zone for all the specimens along with the schematic infographic illustrations consisting of different layers of each micrograph image. The schematic graphs have been drawn manually on the basis of the different contrast as well as different grain shape and size in the image quality. It can be seen that in the sample C27-DQ, the depth of the layers which have plastically deformed i.e. both severely and highly deformed layers are smaller than for the samples which had the equiaxed grain structure (C27-860 and 960). This could be an indication of the lower work hardening capability of the elongated structure compared to the equiaxed structure. However, the EBSD measurements have been obtained from a small area of each sample, and the results could be different for the other regions of the samples. Nevertheless, the sample C27-860 showed the highest depth for the severely and highly deformed layers, though this was not clearly seen in the cross-sectional FESEM images by visual inspection. It is worth mentioning that this sample also had the finest prior austenite grain size and subsequently the highest impact toughness values.
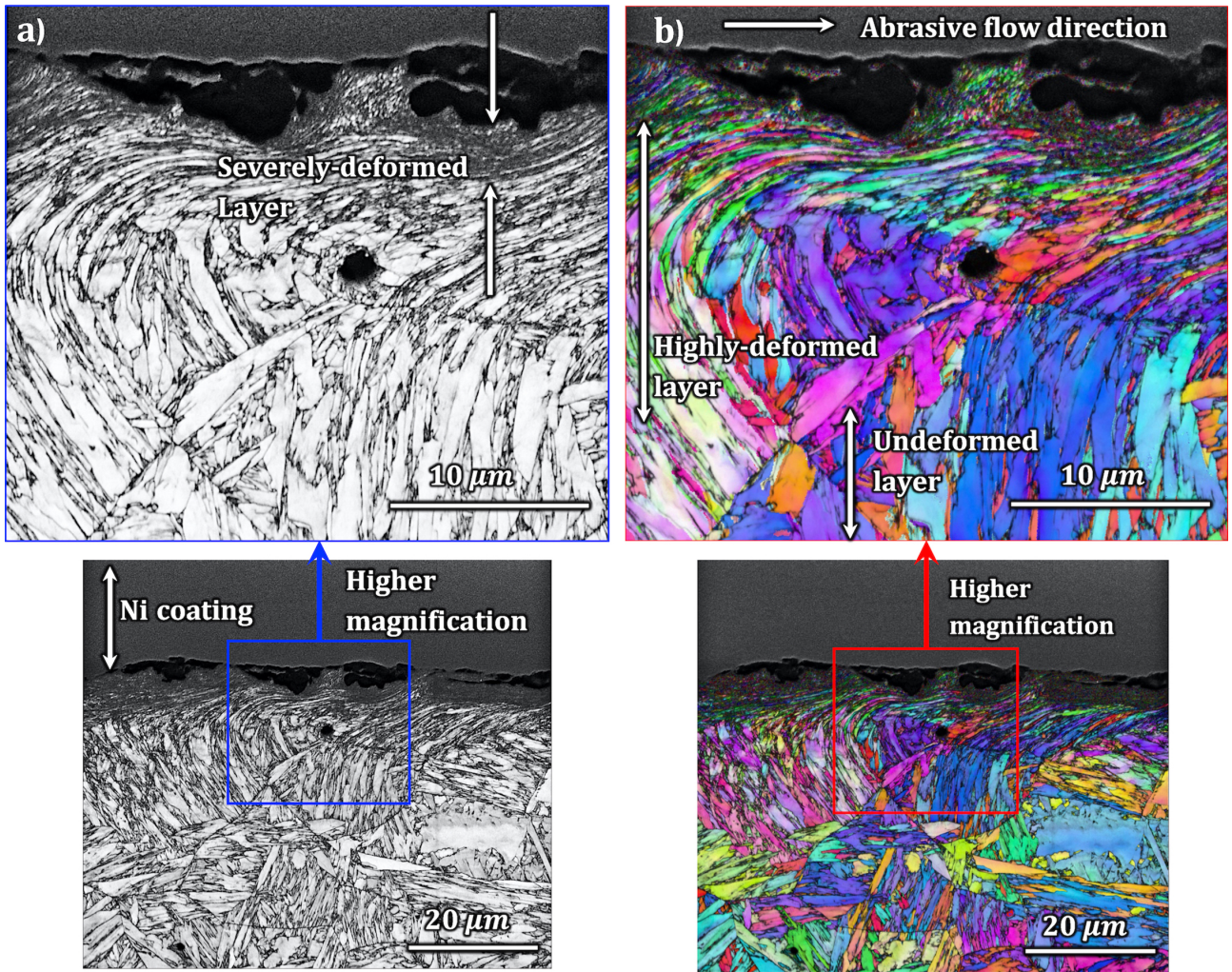
Fig. 11. EBSD imaging of C27-960: a) image quality and b) inverse pole figure map, in two different magnifications.
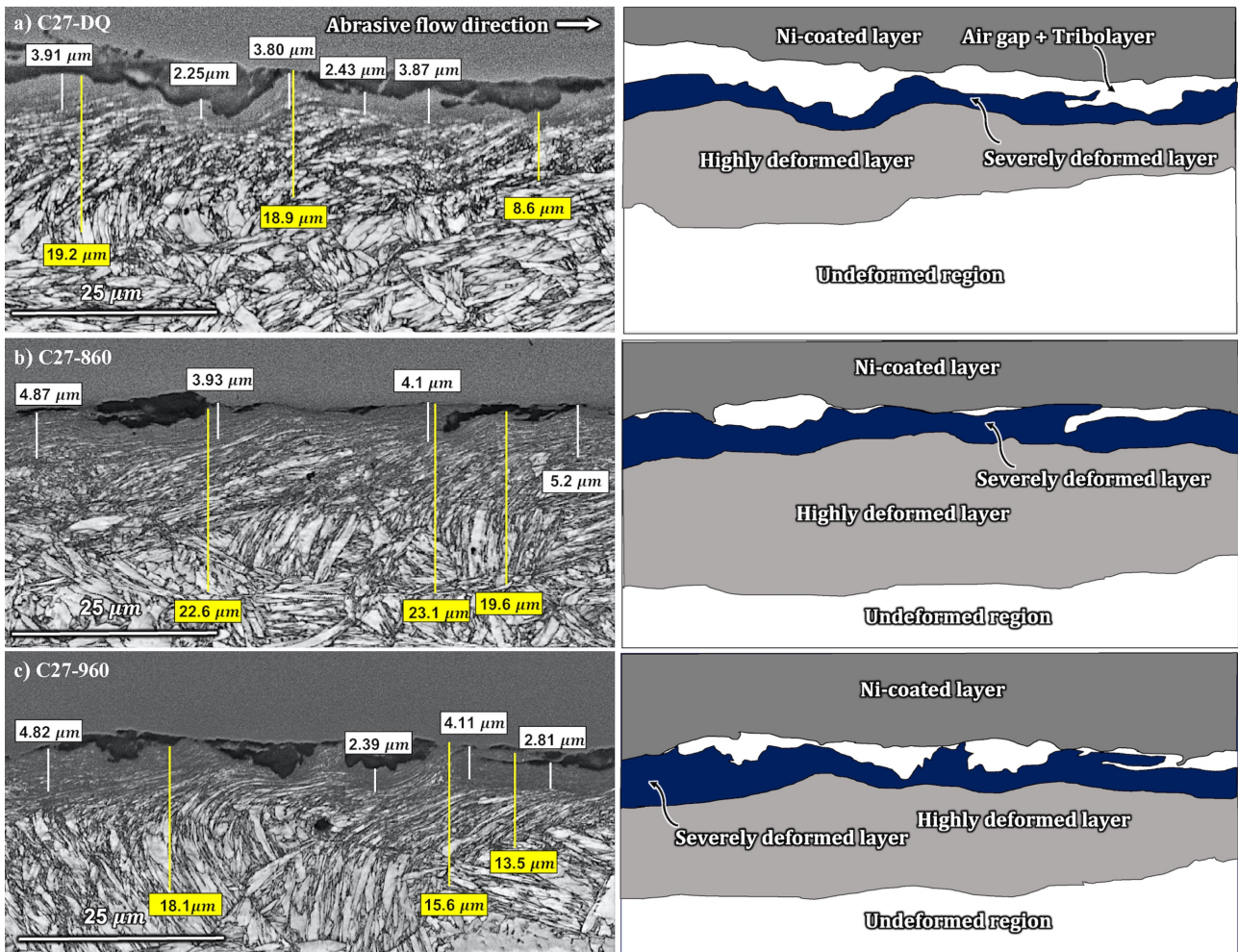
Fig. 12. Image quality figures for the tested samples (left) with schematic illustrations of the wear surface regions with different degrees of deformation.

The EBSD measurements were carried out further with different magnifications for observing the microstructure of the wear surfaces of the samples. The microstructure in the surface layer had transformed into very fine, even to nanoscale cell-like structure. As an example, the results for the C27-DQ sample are given in Fig. 13. The higher magnification revealed that the earlier shown severely deformed layer (see Fig. 12) shows very fine equiaxed grains, whereas the highly deformed layer has deformed and elongated grain structure. The extreme grain refinement indicates that the closest region to the surface, with depth of only 1 or 2 μm, has exhibited formation of new grains.
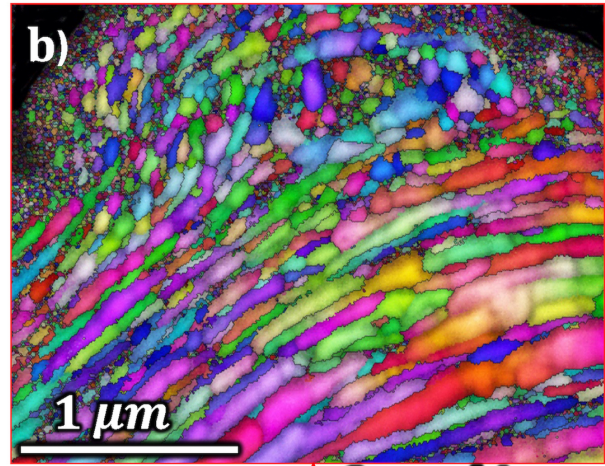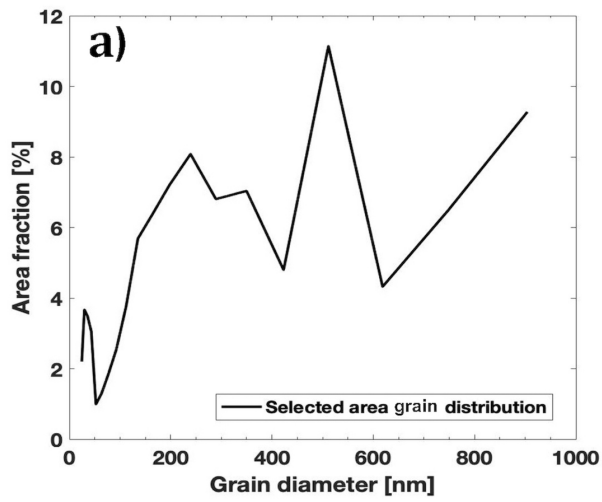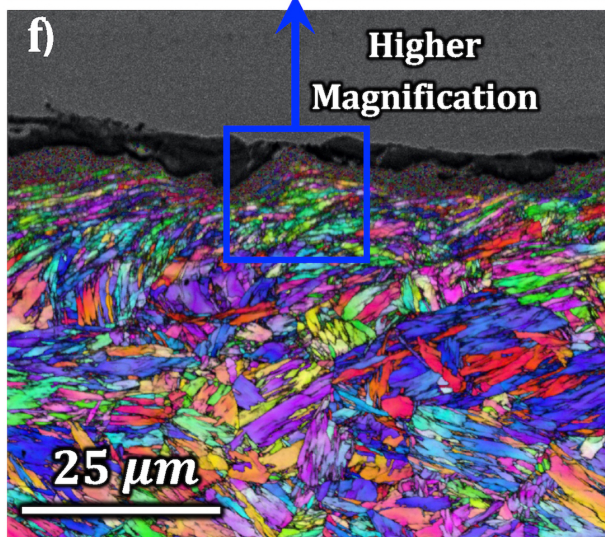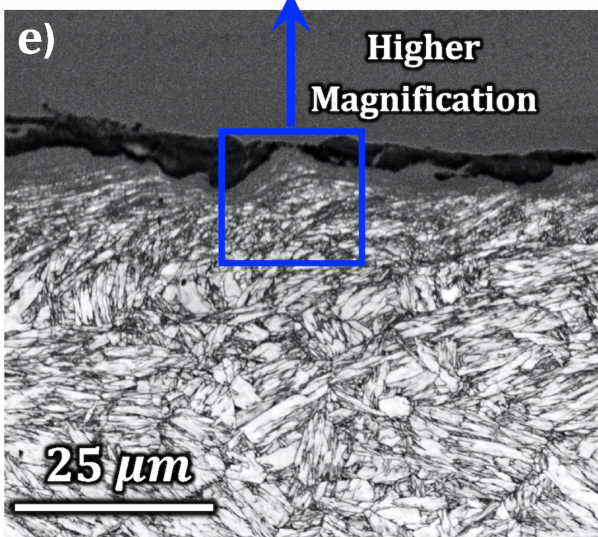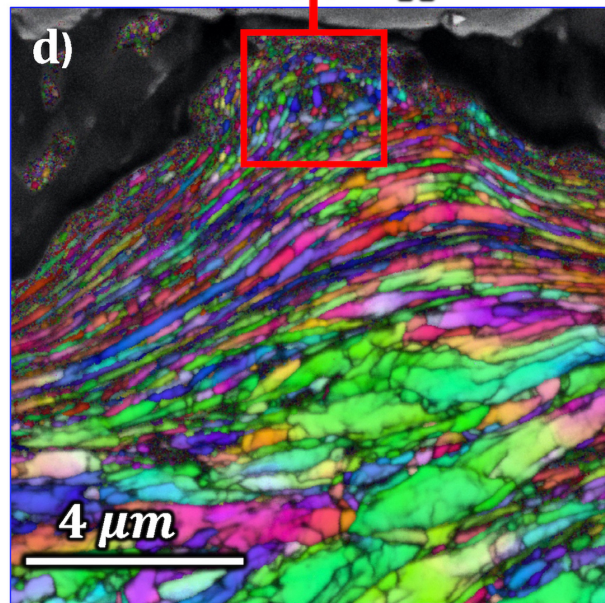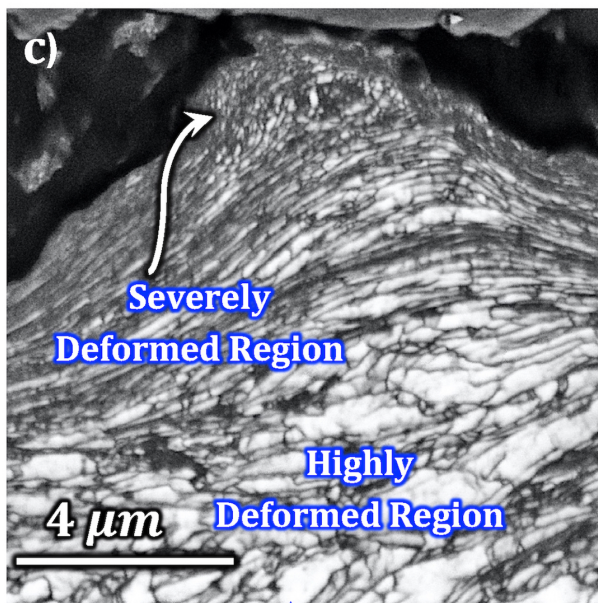
Fig. 13. High resolution images of the cross-section of the wear surface of the C27-DQ sample: a) grain distribution map of a selected area (Fig.13b), b) selected area on the with an almost nanosized grain structure (inverse pole figure), c-f), image quality (c and e), and inverse pole figure map (e and f) at two different magnifications.

4. Discussion

The reaustenitization of a commercial wear-resistant steel, abbreviated C27, resulted in different prior austenite grain sizes, which was expected to influence the abrasive wear resistance of the steels. The subsequent heat treatments of the C27-DQ steel at temperatures of 860 and 960 °C resulted in two steel variants with significantly different prior austenite grain sizes. The temperature increase of 100 °C during the reaustenitization caused the mean linear intercept to increase from 14 μm (C27-860) to 34 μm (C27-960). The grain structure produced with the reaustenitization was much more equiaxed in comparison to the as-received steel. The highly elongated grain structure of the C27-DQ steel (aspect ratio above 2) and the nearly equiaxed C27-860 with almost the same mean linear intercept showed different wear performance in the dry-pot testing. As the initial bulk hardness was very close to each other, the differences in the grain structure and morphology can be considered a possible explanation for the wear test results. The C27-860 had very high hardness after the testing, i.e. greater work-hardening had occurred. Therefore, the results from the dry-pot testing suggest that the hardness of the deformed wear surface, not the initial hardness, correlates better with the abrasive wear resistance of the given steel. However, the mechanisms of the improved word-hardening may now be attributed to the change in the grain size and morphology, as the steels had the same composition and initial hardness. The as-received C27-DQ had slightly higher strength than the two other variants, but it had lower impact toughness compared with the C27-860. However, the C27-960 had the lowest Charpy-V impact energies of the C27 steels and therefore the impact toughness cannot solely explain the results, as also seen earlier with some high-hardness steels [38]. Even though the smaller PAGS has been proposed as one of the plausible reasons for wear-resistant steels having less work-hardening capability during abrasive testing [20] the mentioned work was carried out for commercial steels with similar hardness but different composition. Hence, the steel composition and some alloying elements, such as nickel and molybdenum, could also have significant role in the work-hardening of the steel surface when subjected to abrasion [14,20]. Also, elongation values improved slightly by the reaustenitization, which might improve work-hardening capability. In the current study, the steel samples were initially cut from the same heavy sheet minimizing the differences in alloying element content, though local fluctuations in the composition are always possible.

The texture and grain structure of the surface might be another explanation for the higher mass loss of the as-received C27. The images for the grain size calculations were taken from quarter depth of the thickness of the steel samples to avoid any possible abnormalities caused by surface decarburization (surface) or segregation (middle of the sample). Hence, the surface of the C27-DQ might have had different properties for both the texture and grain structure in comparison to the C27-860 and C27-960. The austenitization conducted for the other two C27 steel variants could have also caused different surface hardness and further altered the initial properties of the steel surface. However, the samples were prepared in similar manner by removing the surface layer by grinding and polishing. Also, the majority of the mass loss during the testing is caused by the rounding of the samples, i.e. the material removal is concentrated on the edges of the sample [20]. Moreover, the initial surface of the samples is altered and removed very rapidly in the beginning of the test. Therefore, it can be assumed that the properties of the bulk material, rather than the initial properties of the surface, determine the material removal rate in the long-lasting wear tests. The EBSD measurements of the samples also confirmed the random-oriented grain structure with no observable texture.

The FESEM imaging showed the strong plastic deformation of the wear surfaces, but more thorough information was extracted with the use EBSD measurements. The cell-like, almost nanoscale structure visible in the FESEM was confirmed to be ultra-fine grain structure by the high quality EBSD mapping. At certain point very near to the surface, the microstructure did not show deformed,

elongated structure, but rather newly formed grains. The size of the grains appeared to decrease closer to the surface, and grains with diameter of 20 nm to1 μm were discovered near the surface. A plausible explanation for the fine grain structure is the strain-induced transformation occurring during the high-stress abrasion. The structure of the surface layer showed similarities to deformed shear bands with some ultra-fine grains [36]. It has been reported that the formation of new grains due to the severe plastic deformation is different from the phenomenon that normally takes place during hot deformation, i.e. conventional dynamic recrystallization on the basis of nucleation and long-range migration of grain boundaries. As Sakai et al. [39] proposed, the mechanism of such a fine grain structure during severe plastic deformation, is combination of original grains' fragmentation along with transformation of deformation bands into high-angle boundaries due to increase in the number of misorientations between shear bands under repeated severe impingements. It is unclear whether this type of plastic deformation occurs during the abrasive high-stress wear, but the current EBSD results suggest some type of similar grain formation.

The EBSD results also showed some differences between the steels, though only one section of each steel was examined. The conducted EBSD analysis suggested that the grain structure possibly affects the work-hardening behavior, and furthermore results in the formation of layers with different degree of plastic deformation. In other words, the depth of the total deformation is not the only factor regarding the work-hardening, but also the severity of the plastic deformation at different depths beneath the wear surface. The deformed layer discovered in the EBSD measurements was divided into two layers, severely and highly deformed regions (Fig. 12), but the higher magnifications revealed that the deformed layer could be divided even further into separate regions (Fig. 13). Now, the emphasis should be on examining and understanding how these layers affect the work-hardening and wear resistance of steels. The deformed layer beneath the wear surface has been discussed in earlier studies. Ojala et al. [14] noted that the transition from the severely deformed layer to the bulk material should be smooth to prevent sharp gradients of hardened surface layer and unworn material. Lindroos et al. [40] emphasized the importance of work-hardening in improving the abrasive wear resistance, but the authors also claimed that the surface-bulk interface could act as pathway for crack propagation, especially under repeated loadings. The extreme hardness of the wear surface might not provide increased wear resistance, if the layer becomes too brittle leading to delamination. The C27-860 in the current tests showed the highest initial and deformed hardness, but also the highly deformed layer was thicker compared to the other two samples. It cannot be clearly stated, whether the depth of the deformed layer and the hardness increase of the wear surface are linked, but presumably these two features combined resulted in the improved wear resistance of the C27-860 over the two other variants.

Though the results indicated that the grain size, or more importantly the grain size, structure, and morphology together, could be a major factor for the abrasive wear resistance of the tested steels by having an effect on the work-hardening, it should be noted that the as-received C27-DQ might have been subjected to low-temperature tempering. This could not be confirmed from neither the laser-optical nor the FESEM microscope images, but the amount of precipitates suggested that either strong autotempering or separate tempering treatment had taken place. Tempering could have had an effect on the wear resistance as seen in earlier work [25], and the possible effects of tempering on the wear resistance of C27-DQ cannot be ruled out. Therefore, to minimize all the variables in future work, steel compositions should be designed for a given subject to study. The challenge is to have minimum amount of alloying content for minimizing the effect of different elements on the work-hardening capability and subsequently on the wear characteristics.

Future work will be carried out to enhance the EBSD imaging of wear surfaces. The current results were first of a kind in terms of image quality when imaging worn steel surfaces. More work will be done to improve the image quality even further, and higher magnifications will be used if possible.

5. CONCLUSIONS

In this study, a commercial 500 HB grade wear-resistant steel was reaustenitized at two different temperatures for examining the effect of prior austenite grain size on the mechanical properties and abrasive wear performance. A total of three steel variants with different prior austenite grain sizes and grain morphology were tested and characterized. The following observations were made:

(1) The reaustenitization at 860 and 960 °C resulted in equiaxed grain structure with 14 μm and 34 μm mean liner intercept values, respectively. The sample in the as-received condition had highly elongated grain structure with aspect ratio over 2 and mean linear intercept of 15 μm. In terms of mechanical properties, the grain size had the most significant effect on the impact toughness: the increase of prior austenite grain size from 14 to 34 μm halved the impact energy when tested at -40 °C with Charpy-V method.

(2) The lowest mass loss in the high-stress abrasive dry-pot testing was measured for the C27-860 sample, which had the smallest prior austenite grain size. Microhardness testing revealed that the C27-860 had the highest surface hardness after wear testing indicating higher work-hardening capability when compared to the other two test variants. FESEM imaging revealed high degree of plastic deformation and orientated structure in the vicinity of the wear surfaces.

(3) The EBSD was successfully utilized to confirm the presence of fine grain structure near the wear surface; an ultra-fine grain structure was discovered near the tribolayer. The depth and severity of the deformed microstructure varied between the steels. The layers were divided into severely and highly deformed regions. The thickness of both layers was the highest for the C27-860, which could explain the best wear performance.

ACKNOWLEDGEMENTS

REFERENCES

[1] G. Krauss, Martensite in steel: strength and structure, Mater. Sci. Eng. A. 273–275 (1999) 40–57. doi:10.1016/S0921-5093(99)00288-9.

[2] J. Zhao, Z. Jiang, Thermomechanical processing of advanced high strength steels, Prog. Mater. Sci. 94 (2018) 174–242. doi:10.1016/j.pmatsci.2018.01.006.

[3] P. Kantanen, M. Somani, A. Kaijalainen, O. Haiko, D. Porter, J. Kömi, Microstructural

Characterization and Mechanical Properties of Direct Quenched and Partitioned High-Aluminum and High-Silicon Steels, Metals (Basel). 9 (2019) 256. doi:10.3390/met9020256.

[4]   A.J. Kaijalainen, P.P. Suikkanen, T.J. Limnell, L.P. Karjalainen, J.I. Kömi, D.A. Porter, Effect of austenite grain structure on the strength and toughness of direct-quenched martensite, J. Alloys Compd. 577 (2013) S642–S648. doi:10.1016/j.jallcom.2012.03.030.

[5]   A.J. Kaijalainen, P. Suikkanen, L.P. Karjalainen, J.J. Jonas, Effect of Austenite pancaking on the microstructure, texture, and bendability of an ultrahigh-strength strip steel, Metall. Mater. Trans. A Phys. Metall. Mater. Sci. 45 (2014) 1273–1283. doi:10.1007/s11661-013-2062-7.

[6]   O. Haiko, M. Somani, D. Porter, P. Kantanen, J. Kömi, N. Ojala, et al., Comparison of impact-abrasive wear characteristics and performance of direct quenched (DQ) and direct quenched and partitioned (DQ&P) steels, Wear. 400–401 (2018) 21–30. doi:10.1016/j.wear.2017.12.016.

[7]   E.O. Hall, The Deformation and Ageing of Mild Steel: III Discussion of Results, Proc. Phys. Soc. Sect. B. 64 (1951) 747–753. doi:10.1088/0370-1301/64/9/303.

[8]   N.J. Petch, The cleavage strength of polycrystals, Journal of Iron and Steel Institute, J. Iron Steel Inst. 174 (1953) 25–28. http://ci.nii.ac.jp/naid/10019881123/en/ (accessed February 18, 2020).

[9]   C. Wang, M. Wang, J. Shi, W. Hui, H. Dong, Effect of microstructural refinement on the toughness of low carbon martensitic steel, Scr. Mater. 58 (2008) 492–495. doi:10.1016/j.scriptamat.2007.10.053.

[10]   C. Zhang, Q. Wang, J. Ren, R. Li, M. Wang, F. Zhang, et al., Effect of martensitic morphology on mechanical properties of an as-quenched and tempered 25CrMo48V steel, Mater. Sci. Eng. A. 534 (2012) 339–346. doi:10.1016/j.msea.2011.11.078.

[11]   C. Ouchi, Development of steel plates by intensive use of TMCP and direct quenching processes, ISIJ Int. 41 (2001) 542–553. doi:10.2355/isijinternational.41.542.

[12]   Y. Prawoto, N. Jasmawati, K. Sumeru, Effect of Prior Austenite Grain Size on the Morphology and Mechanical Properties of Martensite in Medium Carbon Steel, J. Mater. Sci. Technol. 28 (2012) 461–466. doi:10.1016/S1005-0302(12)60083-8.

[13]   O. Haiko, I. Miettunen, D. Porter, N. Ojala, V. Ratia, V. Heino, et al., Effect of Finish Rolling and Quench Stop Temperatures on Impact-Abrasive Wear Properties of 0.35 % Carbon Direct-Quenched Steel, Tribol. - Finnish J. Tribol. 35 (2017) 5–21. https://journal.fi/tribologia/article/view/59344.

[14]   N. Ojala, K. Valtonen, V. Heino, M. Kallio, J. Aaltonen, P. Siitonen, et al., Effects of composition and microstructure on the abrasive wear performance of quenched wear resistant steels, Wear. 317 (2014) 225–232. doi:10.1016/j.wear.2014.06.003.

[15]   K. Valtonen, K. Keltamäki, V.T. Kuokkala, High-stress abrasion of wear resistant steels in the cutting edges of loader buckets, Tribol. Int. 119 (2018) 707–720. doi:10.1016/j.triboint.2017.12.013.

[16]   N. Ojala, K. Valtonen, A. Antikainen, A. Kemppainen, J. Minkkinen, O. Oja, et al., Wear performance of quenched wear resistant steels in abrasive slurry erosion, Wear. 354–355 (2016) 21–31. doi:10.1016/j.wear.2016.02.019.

[17]   A. Sundström, J. Rendon, M. Olsson, Wear behaviour of some low alloyed steels under combined impact/abrasion contact conditions, Wear. 250 (2001) 744–754. doi:10.1016/S0043-1648(01)00712-8.

[18]   J. Rendón, M. Olsson, Abrasive wear resistance of some commercial abrasion resistant steels evaluated by laboratory test methods, Wear. 267 (2009) 2055–2061. doi:10.1016/j.wear.2009.08.005.

[19]   B. Narayanaswamy, P. Hodgson, H. Beladi, Comparisons of the two-body abrasive wear behaviour of four different ferrous microstructures with similar hardness levels, Wear. 350–351 (2016) 155–165. doi:10.1016/j.wear.2016.01.013.

[20] K. Valtonen, N. Ojala, O. Haiko, V. Kuokkala, Comparison of various high-stress wear conditions and wear performance of martensitic steels, Wear. 426–427 (2019) 3–13. doi:10.1016/j.wear.2018.12.006.

[21] I. Sevim, I.B. Eryurek, Effect of fracture toughness on abrasive wear resistance of steels, Mater. Des. 27 (2006) 911–919. doi:10.1016/j.matdes.2005.03.009.

[22] A.R. Chintha, K. Valtonen, V.-T. Kuokkala, S. Kundu, M.J. Peet, H.K.D.H. Bhadeshia, Role of fracture toughness in impact-abrasion wear, Wear. 428–429 (2019) 430–437. doi:10.1016/j.wear.2019.03.028.

[23] A.R. Chintha, Metallurgical aspects of steels designed to resist abrasion, and impact-abrasion wear, Mater. Sci. Technol. (United Kingdom). 35 (2019) 1133–1148. doi:10.1080/02670836.2019.1615669.

[24] K. Valtonen, V. Ratia, N. Ojala, V.-T. Kuokkala, Comparison of laboratory wear test results with the in-service performance of cutting edges of loader buckets, Wear. 388–389 (2017) 93–100. doi:10.1016/j.wear.2017.06.005.

[25] O. Haiko, K. Valtonen, A. Kaijalainen, S. Uusikallio, J. Hannula, T. Liimatainen, et al., Effect of tempering on the impact-abrasive and abrasive wear resistance of ultra-high strength steels, Wear. 440–441 (2019) 203098. doi:10.1016/j.wear.2019.203098.

[26] N. Ojala, K. Valtonen, P. Kivikytö-Reponen, P. Vuorinen, P. Siitonen, V.-T. Kuokkala, Effect of test parameters on large particle high speed slurry erosion testing, Tribol. - Mater. Surfaces Interfaces. 8 (2014) 98–104. doi:10.1179/1751584X14Y.0000000066.

[27] O. Seppälä, S. Uusikallio, J. Larkiola, A tool for computer-aided calculation of grain size, in: D. Szeliga, L. Rauch (Eds.), B. Abstr. XXVI Int. Conf. Comput. Methods Mater. Technol. KomPlasTech 2019, ISBN: 978-83-947091-4-3, 2019: pp. 128–130. http://www.aknet.biz.pl/.

[28] T. Nyyssönen, P. Peura, V.-T. Kuokkala, Crystallography, Morphology, and Martensite Transformation of Prior Austenite in Intercritically Annealed High-Aluminum Steel, Metall. Mater. Trans. A. 49 (2018) 6426–6441. doi:10.1007/s11661-018-4904-9.

[29] V. Javaheri, S. Kolli, B. Grande, D. Porter, Insight into the induction hardening behavior of a new 0.40% C microalloyed steel: Effects of initial microstructure and thermal cycles, Mater. Charact. 149 (2019) 165–183. doi:10.1016/j.matchar.2019.01.029.

[30] V. Javaheri, A. Pohjonen, J.I. Asperheim, D. Ivanov, D. Porter, Physically based modeling, characterization and design of an induction hardening process for a new slurry pipeline steel, Mater. Des. 182 (2019) 108047. doi:10.1016/j.matdes.2019.108047.

[31] R. Stechow, I. Ivanova, M. Naveed, S. Weiß, Sample Preparation of Worn Surfaces for EBSD Analysis, Pract. Metallogr. 53 (2016) 352–359. doi:10.3139/147.110401.

[32] K.W. Andrews, Empirical formulae for the calculation of some transformation temperatures, J. Iron Steel Inst. 203 (1965) 721–727.

[33] T. Nyyssönen, Quenching and Partitioning of High-Aluminum Steels, Tampere Univ. Technol. 1451 (2017).

[34] Y. Xu, H.J. Yang, M.A. Meyers, Dynamic recrystallization in the shear bands of Fe–Cr–Ni monocrystal: Electron backscatter diffraction characterization, Scr. Mater. 58 (2008) 691–694. doi:10.1016/j.scriptamat.2007.12.006.

[35] H. Yang, J.H. Zhang, Y. Xu, M.A. Meyers, Microstructural Characterization Of The Shear Bands In Fe-Cr-Ni Single Crystal, 24 (2008) 819–828.

[36] C. Figueroa, R. Schouwenaars, V. Jacobo, A. Ortiz, R. Petrov, L. Kestens, Tribological and Microstructural Characterization of Ultrafine Layers Induced by Wear in Ductile Alloys, Tribol. Online. 11 (2016) 389–395. doi:10.2474/trol.11.389.

[37] S. Singh, Y. Guo, B. Winiarski, T.L. Burnett, P.J. Withers, M. De Graef, High resolution low kV EBSD of heavily deformed and nanocrystalline Aluminium by dictionary-based indexing, Sci. Rep. 8 (2018) 10991. doi:10.1038/s41598-018-29315-8.

[38] O. Haiko, I. Miettunen, D. Porter, N. Ojala, V. Ratia, V. Heino, et al., Effect of Finish rolling

and quench stop temperatures on impact-abrasive wear resistance of 0.35 % carbon direct-quenched steel, Tribologia. 35 (2017).

[39] T. Sakai, H. Miura, X. Yang, Ultrafine grain formation in face centered cubic metals during severe plastic deformation, Mater. Sci. Eng. A. 499 (2009) 2–6. doi:10.1016/j.msea.2007.11.098.

[40] M. Lindroos, K. Valtonen, A. Kemppainen, A. Laukkanen, K. Holmberg, V.T. Kuokkala, Wear behavior and work hardening of high strength steels in high stress abrasion, Wear. 322–323 (2015) 32–40. doi:10.1016/j.wear.2014.10.018.